ELSEVIER

Journal of Power Sources 90 (2000) 95–102

JOURNAL OF POWER SOURCES

www.elsevier.com/locate/jpowsour

Solid-state ^{7}Li NMR studies of inverse spinel $LiNi_xCo_{1-x}VO_4$ cathode materials

Peter P. Chu [a,*], D.L. Huang [b], George T.K. Fey [b]

[a] *Department of Chemistry, National Central University, Chung-Li, Taiwan 320*
[b] *Department of Chemical Engineering, National Central University, Chung-Li, Taiwan 320*

Received 14 November 1999; received in revised form 25 January 2000; accepted 10 February 2000

Abstract

Solid-state ^{7}Li NMR spectroscopy revealed different Ni/Co distributions in an inverse spinel structure of $LiNi_xCo_{1-x}VO_4$ cathode materials prepared by either a high-temperature solid-state reaction method (abbreviated as the HT method) or a low-temperature solution co-precipitation method (abbreviated as the LT method). Solid-state ^{7}Li NMR measurements confirmed that the lithium nuclear spin was dominated by a chemical shift anisotropy (CSA) interaction compounded with a small second-order quadrupolar interaction. Ni/Co distribution and inhomogeneity of chemical shift tensors (δ_{CSA} and η_{CSA} constants) associated with crystalline defects are accountable for the variation in spread of the MAS spinning side-band manifolds between nickel uptake and preparation methods. The NMR study also revealed that the HT method yielded broader Ni/Co distributions with greater lithium defects, while the LT method gave much more homogeneous Ni/Co distributions with smaller defects. The NMR results were consistent with XRD data that showed a gradual expansion in the unit-cell lattice with increasing Co content. All cells suffered a large irreversible loss in overall capacity in the first cycle and became stable in terms of cycle efficiency during later cycling. We have found that $LiNi_xCo_{1-x}VO_4$ cathode materials prepared by the LT method with more homogeneous Ni/Co distribution and smaller crystalline defects offer a small advantage in capacity over the HT method.

Keywords: Solid-state ^{7}Li NMR spectroscopy; HT method; LT method

1. Introduction

New systems of cathode materials such as $LiNiVO_4$ and $LiCoVO_4$ inverse spinel materials have attracted attention for their unusually high voltage behavior when used in rechargeable lithium batteries [1–5]. Three major systems of high voltage cathode materials are currently available for commercial lithium–ion cells: (1) $LiCoO_2$ by Sony Energytec, (2) $LiNiO_2$ by Moli Energy (1990), and (3) $LiMn_2O_4$ by Bellcore. Both $LiCoO_2$ and $LiNiO_2$ possess a layered structure while $LiMn_2O_4$ has a spinel structure. The upper voltage limits of these three systems are in the 4.1–4.5 V range, whereas the inverse spinels in the present study can sustain a voltage as high as 4.2–4.8 V.

Two methods were previously proposed to prepare the cathode materials. Although compatibility between the electrolyte and anode interface can also affect cell performance, cathode structure is the decisive factor in cell potential and performance. Only a few studies have tried to illustrate the structure and properties of $LiMVO_4$ (M = Ni or Co) inverse spinels and even less attention has been directed toward their battery applications. These studies included general characterization of crystal structure [6,7], magnetic properties [6], infrared spectroscopy [8], phase diagram [9], and electric conductivity [10]. The core structural characteristics would be the types of Li coordination, integrity of the cathode materials, and Ni/Co concentration and distribution, all of which are related to battery performance.

Solid-state ^{7}Li NMR technique is sensitive to local structural change and suitable for monitoring Li environments with varying adjacent metal content. Relevant structural characteristics, such as local bonding geometry, Li–O bond distance, O–Li–O dihedral angle, and local electric field gradient are readily reflected in the ^{7}Li static line

* Corresponding author.
E-mail address: pjchu@rs970.ncu.edu.tw (P.P. Chu).

0378-7753/00/$ - see front matter
PII: S0378-7753(00)00454-7

shapes and MAS spinning side-band manifolds. Generally, line broadening in a static NMR spectrum is caused by chemical shift anisotropy, dipole–dipole interaction and quadrupolar interaction. Although solid-state ^{7}Li NMR spectroscopy is a useful technique for the micro-structural analysis of cathode materials for lithium ion batteries, only a few NMR research papers on the topic have been reported [11–19].

Lithium atoms produced rather complicated MAS spinning side-band manifolds in ^{7}Li NMR spectra. The major tasks in this study were to resolve ^{7}Li ($I = 3/2$) NMR signals, governed by both chemical shift anisotropy and quadrupolar interactions, and to disentangle the interaction between Li coordination and surrounding Ni/Co distribution. These NMR results are compared with prior X-ray studies and factors favorable to cell performance are proposed. The present paper will focus on the analysis of micro-structural details and property relationships.

2. Experimental

$LiNi_xCo_{1-x}VO_4$ ($0 \leqq \times \leqq 1$) samples were synthesized by both the HT and LT methods. Typically, HT–$LiNi_xCo_{1-x}VO_4$ samples were prepared by reacting stoichiometric quantities of Li_2CO_3, NiO, Co_3O_4, and V_2O_5 in air at 800°C for 12 h. LT–$LiNi_xCo_{1-x}VO_4$ samples were prepared by first dissolving stoichiometric quantities of $LiOH \cdot H_2O$, $Ni(NO_3)_2 \cdot 6H_2O$, $Co(NO_3)_2 \cdot 6H_2O$, and NH_4VO_3 in deionized water. After vigorous stirring, a brown gel was formed (the color became darker when Co content was higher) and dried at 150°C for 12 h resulting in a brown precursor. The final product was obtained by heating the precursor at 500°C for 48 h.

NMR experiments were performed using a Bruker DSX-400 (9.4 T) and a DSX-300 (7.5 T) NMR instrument, with a ^{7}Li ($I = 3/2$) resonance frequency of 155.27 and 117 MHz, respectively. A normal $\pi/2$ single-pulse excitation with a square pulse width of 4 μs and a delay time of 1 s were used. The typical number of scans was 600 and aqueous LiCl (0.5 N) solution was used as an external reference. The rotation speed was kept as high as 11 kHz to avoid an overlapping of the spinning side-bands.

Glass test cells were constructed and galvanostatically cycled to the desired depths (usually from 3.0 to 4.5 V or up to 4.7 V) using an Amel model 545 galvanostat-electrometer at a current density of 0.1 mA/cm^2 and using 1 M $LiBF_4$ − EC + PC + DMC (1:1:4) as an electrolyte.

3. Results and discussion

The total ^{7}Li NMR spectrum of $LiNiVO_4$ with a rotation frequency of 11 kHz is shown in Fig. 1c. Equally spaced side-band manifolds concentrated around 0.0 ppm are attributed to the ($-1/2$ to $1/2$) central transition. The near mirror-image of the satellite lines correspond to the singularity and shoulders of the ($1/2$ to $3/2$) and ($-3/2$ to $-1/2$) satellite transitions are indicated in Fig. 1d of the theoretical static powder spectrum according to the first order quadrupolar interaction [11]. From the singularity occurring at 500 kHz, (Fig. 1d), the electric field gradient (e.f.g.) tensor was found to be nearly axially symmetrical ($\eta_Q = 0$) with $e^2qQ = 667$ kHz according to the relationship

$$e^2qQ = \frac{2}{3}\nu_Q hI(2I-1) \quad (1)$$

where I = nuclear spin operator, h = Planck's constant, ν_Q = quadrupole frequency.

Comparing the total pattern at two different fields, we have found that the spread of side-band increased linearly with magnetic field strength, indicating that anisotropy is originated from the first-order interaction [19]. However, the only first-order interaction still existing in the central transition ($1/2$ to $-1/2$) is the chemical shift anisotropy δ_{CSA} since quadrupolar interaction contributes only to the second order. A blow-up of the ($-1/2$ to $1/2$) central transition portion (Fig. 1b) of the total spectrum reveals

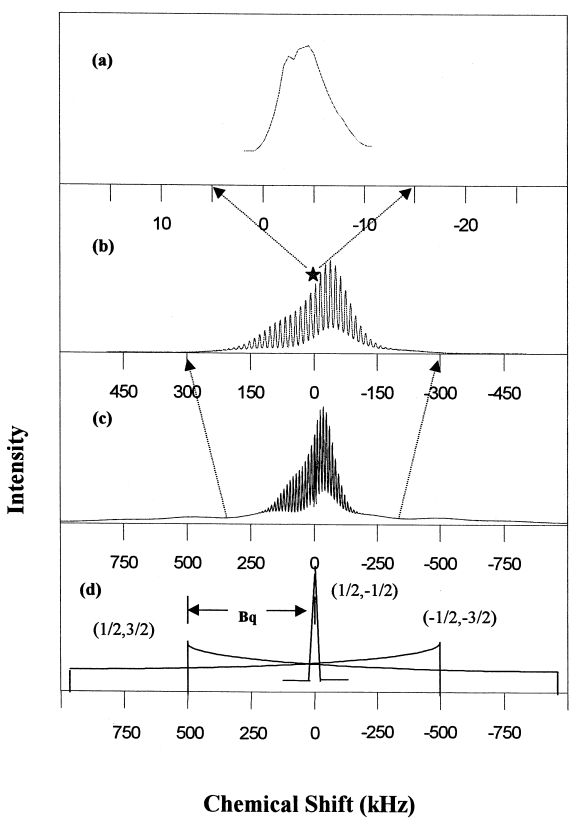

Fig. 1. Total ^{7}Li NMR spectra of $LiNiVO_4$ with rotating frequency $\nu_r = 11$ kHz. (a) A surviving second-order central transition, (b) a blow-up of the central transition, (c) total spectrum, (d) static powder pattern of $3/2$ spin quadrupolar nuclei.

that the side-band manifold is distributed asymmetrically, confirming that the pattern is governed by the chemical shift interaction with an anisotropy δ_{CSA} of about 257 kHz and η_{CSA} near 0.7. From the location of singularities in the satellite transitions, the quadrupolar interaction tensor is calculated to be nearly axially symmetric with e^2qQ near 667 kHz. Further expansion of the center band of central transition located near 0 ppm (Fig. 1a) reveals a residue line width of 6 kHz, which represents the effect caused by the second-order quadrupolar interaction ($H_q^{(2)} = 24$ kHz). This value is negligible compared to the spread of MAS side-bands and its effect on side-band intensity is small. The following discussion will be focused on the change of CSA with structure and nickel content based on the understanding that e.f.g. contributes negligibly to the MAS side-band manifold.

With more cobalt substitution, the residual line width became even smaller, reflecting even smaller quadrupolar interaction than the $x = 1.0$ case described previously. The side-band patterns of the ^{7}Li central transition for $LiNi_xCo_{1-x}VO_4$ samples prepared by the HT method are shown in Fig. 2. The side-band manifolds that were modulated mainly by chemical shift anisotropy reached as far as ± 200 kHz, but the residual line width of each side-band was still narrow compared to the side-band separation of 11 kHz (the spinning rate). With the locations of the three

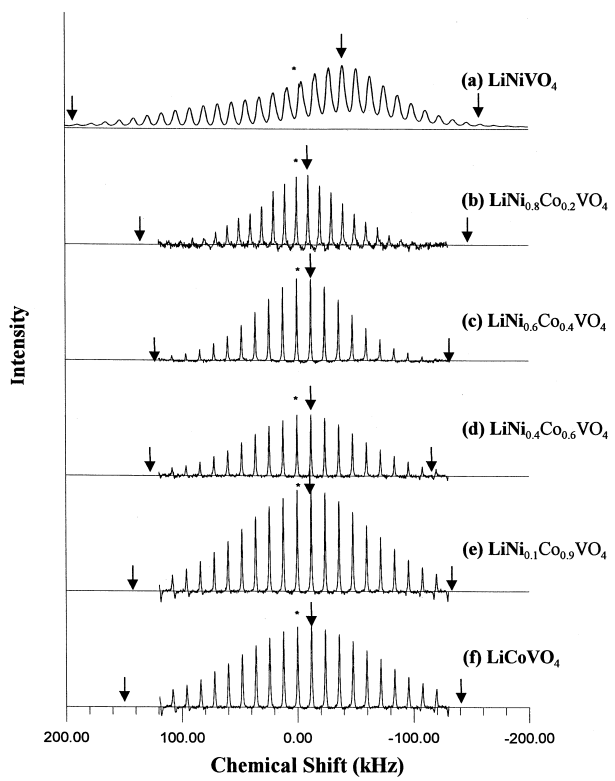

Fig. 2. Superposition of the MAS side-band manifolds for $LiNi_xCo_{1-x}VO_4$ samples prepared by the HT method at various x stoichiometries.

singularities identified, the anisotropy and asymmetry can be calculated following the relationships,

$$\delta_{CSA} = \delta_3 - \frac{\delta_1 + \delta_2}{2} \quad (2)$$

$$\eta_{CSA} = \frac{\delta_2 - \delta_1}{\delta_3 - \delta_{ISO}} \quad (3)$$

$$\delta_{ISO} = \frac{1}{3}(\delta_1 + \delta_2 + \delta_3) \quad (4)$$

where δ_1, δ_2, δ_3, are the principal components of chemical shift tensors.

It can be estimated that the e^2qQ values for the rest of the samples are smaller than 667 kHz, consistent with the understanding that lithium is a very weak quadrupolar nuclei ($Q \ll 0.002$) whose quadrupolar coupling constant remains small, even at strong electric field gradients e^2qQ. The lack of multiple overlapped groups of side-bands indicated that only a single lithium coordinated species was present. The nearly axially symmetrical CSA and e.f.g. tensor suggested that all lithium are octahedrally coordinated, consistent with an inverse spinel structure. By replacing more Ni with Co, spread of side-bands decreased first and increased again with further increases in Co content, a direct indication that chemical shift anisotropy was larger in the beginning and initially decreased first and followed by a rapid increase. Changes in the Ni/Co ratio appeared to initiate structural changes as reflected by changes in the CSA.

The MAS spinning side-band manifold of the Li central transition for $LiNi_xCo_{1-x}VO_4$ samples prepared by the LT method is displayed in Fig. 3. Similar to the HT-sample, a large spread in the MAS side-band manifold was observed due to the size of δ_{CSA}. Again, the CSA was largest in the beginning at low Co content, decreased first, and then increased with increasing Co content. The main difference between these two series was that the LT-sample showed apparently smaller δ_{CSA} than the HT-sample.

Furthermore, upon closer examination of the MAS side-band intensity, the pattern was not reminiscent of any known CSA asymmetry. The greatest discrepancy appeared in the tail of the high spinning side-band intensity which did not decrease sharply, but only tapered down gradually. The three interaction parameters δ_{iso}, δ_{CSA} and η_{CSA} can be derived by combining analysis of the wide-line static NMR powder pattern and the side-band multiple intensities at high rotation speed under magic angle ($\nu_r = 11$ kHz).

Table 1 summarized the fitting results of various Ni/Co ratios using a simple lattice model for the LT and HT samples. To better visualize the trends in these quadrupolar interaction parameters, Figs. 4 and 5 show the variation of η_{CSA} and δ_{CSA} with Ni content deduced from the prescribed MAS side-band analysis. For the LT samples, with

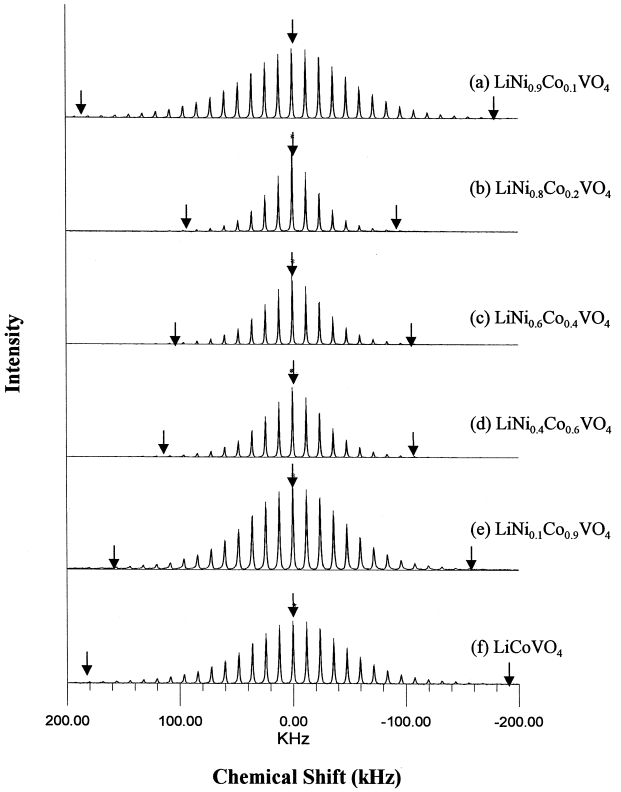

Fig. 3. Superposition of the MAS side-band manifolds for $LiNi_xCo_{1-x}VO_4$ samples prepared by the LT method at various x stoichiometries.

increasing Ni fraction, the δ_{CSA} first decreased from 293 kHz ($x = 0$) to 150 kHz ($x = 0.8$) followed by an increase to 283 kHz ($x = 0.9$). The asymmetry η_{CSA} remained nearly 0.9 to 1.0 for all compositions. The isotropic chemical shift, δ_{ISO}, remained nearly 1.3 ppm. These results are consistent with the randomly distributed Ni and Co in the octahedral cage. $[Ni]_{oh}$ did not appear clustered in the sample prepared by the LT method. We have deduced the three quadrupolar interaction parameters of the HT method as shown in Table 1. The trends are also overlaid with LT samples in Fig. 3 for better visualization. The results

Table 1
^{7}Li NMR characteristics of $LiNi_xCo_{1-x}VO_4$ prepared by either the HT or LT method

$LiNi_xCo_{1-x}VO_4$	Methods					
	HT method			LT method		
	δ (ppm)	δ_{CSA} (kHz)	η_{CSA}	δ (ppm)	δ_{CSA} (kHz)	η_{CSA}
$LiCoVO_4$	1.27	225	0.87	1.35	293	0.97
$LiNi_{0.1}Co_{0.9}VO_4$	1.42	210	0.86	1.33	240	0.94
$LiNi_{0.4}Co_{0.6}VO_4$	1.13	195	0.85	1.35	180	0.92
$LiNi_{0.6}Co_{0.4}VO_4$	1.24	165	0.82	1.33	158	0.90
$LiNi_{0.8}Co_{0.2}VO_4$	1.28	135	0.77	1.34	150	0.90
$LiNi_{0.9}Co_{0.1}VO_4$	–	–	–	1.35	283	0.92
$LiNiVO_4$	−2.13	300	0.60	–	–	–

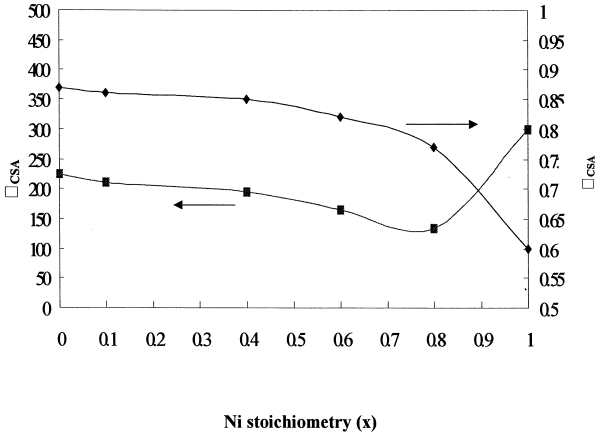

Fig. 4. Variation of η_{CSA} and δ_{CSA} with Ni stoichiometry (x) deduced from the MAS side-band analysis for $LiNi_xCo_{1-x}VO_4$ prepared by the HT method (η_{CSA} ■◇ and δ_{CSA} ■ △).

suggested that with increasing Ni fraction, δ_{CSA} decreased from 225 kHz ($x = 0$) to 135 kHz ($x = 0.8$), followed by a rapid increase to 300 kHz ($x = 1.0$). The asymmetry η_{CSA} decreased from 0.87 ($x = 0$) to 0.77 ($x = 0.8$), then decreased to 0.6 ($x = 1.0$) while the chemical shift δ_{ISO} gradually decreased from 1.42 ppm ($x = 0.1$) to 1.3 ppm ($x = 0.4$), then steadily increased to 1.28 ppm ($x = 0.8$) except when $LiCoVO_4$ ($x = 0$) and $LiNiVO_4$ ($x = 1$). The effective e^2qQ values were larger and the asymmetry change greater than LT samples with the same compositions. Interestingly, we also noted a narrower line width in the medium Ni/Co regime for both LT and HT samples. The change in spread cannot be explained solely by the Ni/Co distribution, since in the pure Ni and Co case, where such issues were absent, we have also observed a reduction in the spread of MAS side-band changing from HT to LT samples. The Ni and Co distribution in the HT-samples was not as random as in the LT-samples, but showed increasingly inhomogeneous distribution with increasing Ni fraction. The line width being the narrowest,

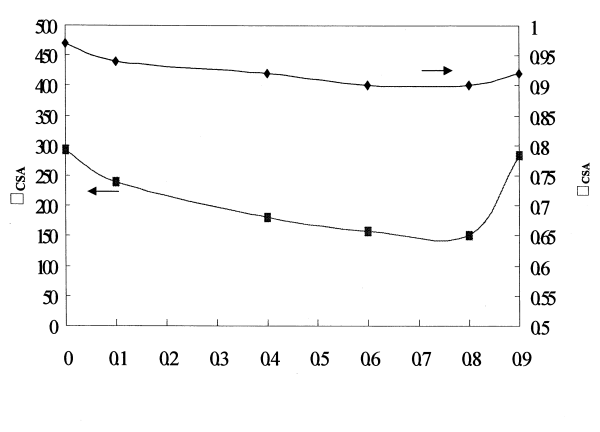

Fig. 5. Variation of η_{CSA} and δ_{CSA} with Ni stoichiometry (x) deduced from the MAS side-band analysis for $LiNi_xCo_{1-x}VO_4$ prepared by the LT method (η_{CSA} ■◇ and δ_{CSA} ■ △).

Table 2
Elemental analysis from ICP-AES for $LiNi_xCo_{1-x}VO_4$ prepared by (a) the HT method; (b) the LT method

Theoretical values	Experimental ICP-AES values	
	(a) HT method	(b) LT method
$LiCoVO_4$	$Li_{0.92}Co_{0.97}VO_4$ ($Li_{0.92}Ni_{0.97}VO_{3.93}$)	$Li_{0.93}Co_{0.95}VO_4$ ($Li_{0.93}Co_{0.95}VO_{3.92}$)
$LiNi_{0.1}Co_{0.9}VO_4$	$Li_{0.93}Ni_{0.11}Co_{0.89}VO_4$ ($Li_{0.93}Ni_{0.11}Co_{0.89}VO_{3.97}$)	$Li_{0.95}Ni_{0.09}Co_{0.93}VO_4$ ($Li_{0.95}Ni_{0.09}Co_{0.93}VO_{4.0}$)
$LiNi_{0.4}Co_{0.6}VO_4$	$Li_{0.92}Ni_{0.41}Co_{0.60}VO_4$ ($Li_{0.92}Ni_{0.41}Co_{0.60}VO_{3.97}$)	$Li_{0.94}Ni_{0.32}Co_{0.66}VO_4$ ($Li_{0.94}Ni_{0.32}Co_{0.66}VO_{3.95}$)
$LiNi_{0.6}Co_{0.4}VO_4$	$Li_{0.91}Ni_{0.62}Co_{0.38}VO_4$ ($Li_{0.91}Ni_{0.62}Co_{0.38}VO_{3.95}$)	$Li_{0.94}Ni_{0.60}Co_{0.38}VO_4$ ($Li_{0.94}Ni_{0.60}Co_{0.38}VO_{3.95}$)
$LiNi_{0.8}Co_{0.2}VO_4$	$Li_{0.92}Ni_{0.81}Co_{0.20}VO_4$ ($Li_{0.92}Ni_{0.81}Co_{0.20}VO_{3.97}$)	$Li_{0.95}Ni_{0.77}Co_{0.19}VO_4$ ($Li_{0.95}Ni_{0.77}Co_{0.19}VO_{3.75}$)
$LiNi_{0.9}Co_{0.1}VO_4$	$Li_{0.92}Ni_{0.93}Co_{0.10}VO_4$ ($Li_{0.92}Ni_{0.93}Co_{0.10}VO_{3.99}$)	$Li_{0.94}Ni_{0.86}Co_{0.1}VO_4$ ($Li_{0.94}Ni_{0.86}Co_{0.1}VO_{3.93}$)
$LiNiVO_4$	$Li_{0.92}Ni_{0.94}VO_4$ ($Li_{0.92}Ni_{0.94}VO_{3.90}$)	$Li_{0.95}Ni_{0.94}VO_4$ ($Li_{0.95}Ni_{0.94}VO_{3.92}$)

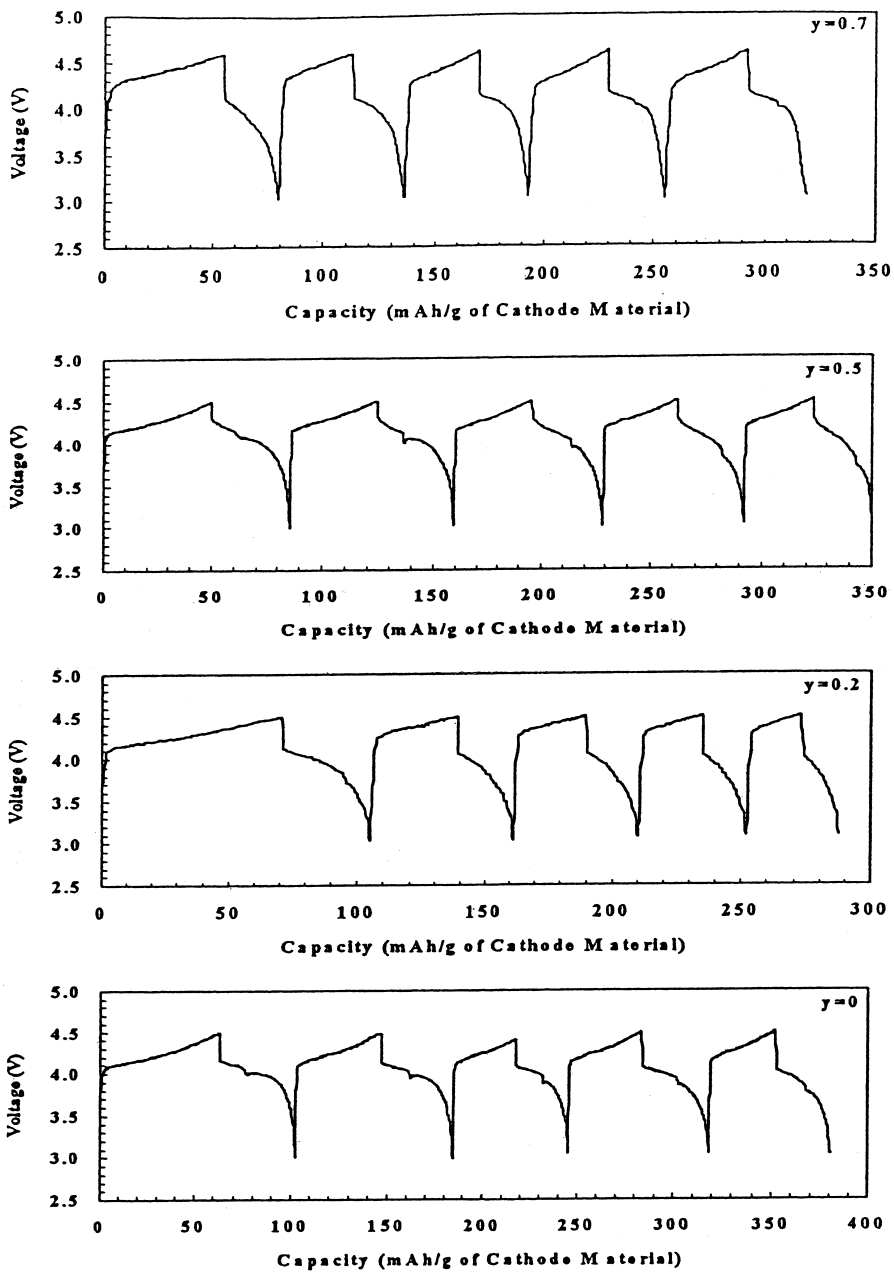

Fig. 6. The charge–discharge curves of Li/1 M $LiBF_4$ − EC + PC + DMC (1:1:4)/$LiNi_xCo_{1-x}VO_4$ cells (where $x = 0$, 0.2, 0.5, or 0.7), whose cathode materials were prepared by the HT method (0.1 mA/cm^2).

and e^2qQ being the smallest in the 80% Ni range may have been due to a more homogeneous distribution of Ni or Co cations in the medium composition range where crystalline and cation defects were both at a minimum.

Elemental analysis by ICP-AES is summarized in Table 2 for the two samples prepared by the HT and LT methods. The composition suggested that the LT method gave an Li:Ni:Co ratio closer to the $1:x:(1-x)$ stoichiometry, although the average Li stoichiometry in each VO_4 cage was about 0.94. On the other hand, the HT method gave rise to a greater deviation from stoichiometry of Li:Ni:Co ratio, where Li content bore an even lower average value of 0.92 for each VO_4 unit. The missing elements created empty octahedral sites where Li, Ni and/or Co were missing. Crystalline defects can be significant in the following three ways: (1) they distort VO_4 symmetry, V–O bond length, and O–V–O bond angles; (2) they create a larger unbalanced electric field leading to a greater electric field gradient at the Li center; and (3) they make more room for Li migration during charge/discharge process. With these assumptions, the changes in MAS profile suggest that the mixed Ni/Co samples $(1 > x > 0)$ contain less crystalline defects than those parent samples ($x = 1$ or $x = 0$) prepared by both the HT and LT methods, and that the LT method gives rise to samples with less crystalline defects than the HT method. The larger δ_{CSA} value observed in the HT samples is related to the larger number of Li deficiencies. However, the smaller δ_{CSA} values in the mixed Ni/Co samples imply that Ni and Co atom distribution must be considered.

Our prior studies showed that the XRD patterns of all mixed Ni/Co samples prepared by either the HT or LT method were very similar to those of their inverse-spinel parent compounds, $LiCoVO_4$ and $LiNiVO_4$. The absence of amorphous domain in the diffraction data indicated that the materials were highly crystalline at all compositions. The diffraction peaks all appeared very sharp, confirming that individual Ni-rich or Co-rich domains did not form. Most interestingly, an almost linear increase in the lattice constant, L''_a from 8.22 A ($x = 1.0$) to 8.28 A ($x = 0$) [4], was detected with increasing Co content for both HT and LT samples, which had different degrees of Li deficiency. If Co and Ni were homogeneously distributed among lattices, there would be no lattice defects. This finding is inconsistent with the fact that Ni has a smaller effective cation radius than Co and that there is a Ni/Co distribution in the lattice. While XRD results indicated that Ni and Co are homogeneously distributed, ^{7}Li NMR data showed that there were significant differences in the microstructure between HT and LT samples due to the fact that Li spin interactions are extremely sensitive to local crystalline defects, while the XRD technique gives bulk-averaged results that fail to provide any information regarding local structural variations.

The inhomogeneity of these materials is partly responsible for their electrochemical behavior in charge/discharge voltage, cell capacity, and cycling efficiency. Fig. 6 shows a comparison of the charge–discharge characteristics of Li/1 M $LiBF_4$ − EC + PC + DMC (1:1:4)/Z cells where Z is either a $LiCoVO_4$ or $LiNi_xCo_{1-x}VO_4$ (where $x = 0$, 0.2, 0.5, or 0.7) cathode material prepared by the HT method. As nickel stoichiometry x increased to 0.8 or above, the cell had to be charged higher than 4.8 V. Undoubtedly, some electrolyte oxidation occurred at such a high voltage causing a rapid decline in capacity during the initial cycle. As a result, we were unable to obtain satisfactory cycling performance for cells with $x = 0.8$, 0.9 and 1.0. Fig. 7 displays the charge and discharge curves of Li/1 M $LiBF_4$ − EC + PC + DMC (1:1:4)/$LiNi_xCo_{1-x}VO_4$ cells (where $x = 0$ or 0.5), which showed similar cell behavior using cathode materials prepared by the LT method.

The capacity data of Li/1 M $LiBF_4$ − EC + PC + DMC (1:1:4)/$LiNi_xCo_{1-x}VO_4$ cells (where $x = 0$ or 0.5) selected from Figs. 6 and 7 are listed in Table 3 for two cathode materials prepared by both the HT and LT methods. In order to be representative, $LiNi_{0.5}Co_{0.5}VO_4$ was selected. In general, the LT method offers a small advantage in capacity over the HT method. All cells suffered a large irreversible loss in overall capacity in the first cycle but cycle efficiency stabilized during cycling.

In samples containing more Co content, both charge and discharge capacities were higher than those in which Ni and Co occupied half of the octahedral sites. The greater crystalline defects in samples where $x = 1$ or $x = 0$ are likely to have a distorted VO_4, making it easier for lithium intercalation/deintercalation. However, when compared to the samples of mixed composition ($x = 0.5$), such structural defects led to lower crystalline free energy and destabilized the framework of the lattice. As a result,

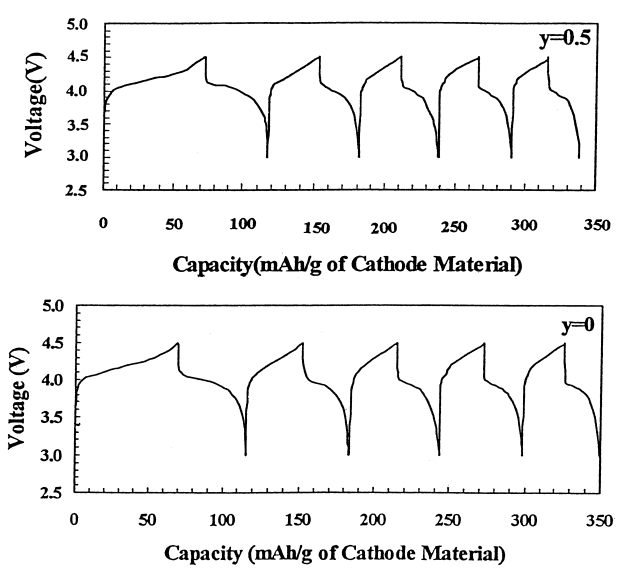

Fig. 7. The charge and discharge curves of Li/1 M $LiBF_4$ − EC + PC + DMC (1:1:4)/$LiNi_xCo_{1-x}VO_4$ cells (where $x = 0$ or 0.5) with cathode materials prepared by the LT method (0.1 mA/cm^2).

Table 3
A comparison of selected capacity data of Li/1 M $LiBF_4$ − EC + PC + DMC (1:1:4)/$LiNi_xCo_{1-x}VO_4$ cells (where $x = 0$ or $x = 0.5$) with cathode materials prepared by either the HT or LT method

Cycle	$X = 0.0$			$X = 0.5$		
	Charge capacity (mA h/g)	Discharge capacity (mA h/g)	Cycle efficiency (%)	Charge capacity (mA h/g)	Discharge capacity (mA h/g)	Cycle efficiency (%)
HT method						
1st	63	40	64	50	35	69
2nd	44	38	86	40	34	85
3rd	33	29	88	37	33	90
4th	38	35	90	34	31	91
5th	33	29	88	40	37	91
LT method						
1st	69	47	67	67	44	65
2nd	36	32	88	34	30	89
3rd	31	28	90	29	26	92
4th	30	26	88	27	25	91
5th	28	24	89	27	25	92

cycling efficiency decreased rapidly as the cycling process continued. In comparison, LT prepared samples with reduced structural defects showed higher cathode material integrity as reflected in the improvement of cycling efficiency. Nevertheless, the initial charge and discharge capacities of LT prepared samples were lower than HT prepared samples.

Invariably, the cathode that gives rise to higher charge voltage shows lower cycle efficiency, a trend consistent with the understanding that samples with greater defects favor Li transference, but may be harmful to sample integrity during cycling. With greater crystalline defects, the cathode structure will soon decay to a metastable configuration during cycling.

4. Conclusions

Solid-state ^{7}Li NMR studies of an inverse spinel structure of $LiNi_xCo_{1-x}VO_4$ cathode materials revealed how the Li environment varied with Ni/Co content. The NMR results (Table 1) indicated that crystalline defects in the inverse spinel structure of $LiNi_xCo_{1-x}VO_4$ have strongly affected charge/discharge voltage, capacity, and cycling efficiency. ^{7}Li NMR analysis of high speed MAS ($\nu_r = 11$ kHz) side-band multiplets showed that major spin interactions are chemical shift anisotropy heavily dependent upon Li–O bond distance and O–Li–O dihedral angle, and revealed that Li defects and Ni/Co distributions are present in the neighboring octahedral cage. The results are consistent with randomly distributed Ni and Co. $[Ni]_{oh}$ did not appear clustered for the sample prepared by the LT method, but in the samples prepared by the HT method, Ni and Co were not distributed as randomly as in the LT prepared samples, but showed increasingly inhomogeneous distribution with increasing Ni fraction.

ICP-AES analysis of the composition of the end-products showed that all compounds were lithium deficient and deviated from the theoretical value of $x = 1$. The result indicated that lithium mass was lost during the heating process, and caused crystalline defects. Larger numbers of crystalline defects in the HT prepared samples gave rise to higher e.f.g. for the remaining lithium, as reflected in the larger spread in the side-band manifolds. These results demonstrated that the LT method produced cathode materials with the most uniform Ni/Co distribution, and that samples prepared by the HT method required annealing to homogenize the Ni/Co distribution. While XRD results indicated that Ni and Co atoms were homogeneously distributed, ^{7}Li NMR data showed that there were significant differences in microstructure between the HT- and LT-prepared samples. The present study has clearly demonstrated that the solid-state NMR technique is capable of deducing the micro-structural information, such as Li coordination and Ni/Co distribution, which is relevant to Li transferability in cathode materials.

Acknowledgements

The financial support of this work was provided by the National Science Council of the Republic of China, under contract nos. NSC-86-2113-M-008-004 and NSC-87-2214-E-008-015. The excellent service of Mrs. Fang Su-yun at Hsin-Chu National Equipment Center in providing NMR measurements is gratefully acknowledged.

References

[1] G.T.K. Fey, W. Li, J.R. Dahn, J. Electrochem. Soc. 141 (1994) 227.
[2] G.T.K. Fey, W.B. Perng, Mater. Chem. Phys. 47 (1997) 279.
[3] G.T.K. Fey, C.S. Wu, J. Pure Appl. Chem. 69 (1997) 329.

[4] G.T.K. Fey, K.S. Wang, S.M. Yang, J. Power Sources 68 (1997) 159.
[5] J.M. Tarascon, D. Guyomard, J. Electrochem. Soc. 138 (1991) 2864.
[6] J.C. Bernier, P. Poix, A. Michel, Bull. Soc. Chim. Fr. (1963) 1661.
[7] G. Blasse, J. Inorg. Nucl. Chem. 25 (1963) 230.
[8] J. Preudhomme, P. Tarte, Spectrochim. Acta A 28 (1972) 69.
[9] Y. Ito, Nippon Kagaku Kaishi 11 (1979) 1483.
[10] Y. Ito, T. Maruyama, T. Nakamura, Y. Saito, Rep. Res. Lab. Eng. Mater., Tokyo Inst. Technol. 11 (1986) 11.
[11] S. Hayakawa, T. Yoko, S. Sakka, Bull. Chem. Soc. Jpn. 66 (1993) 3393.
[12] S. Hayakawa, T. Yoko, S. Sakka, J. Ceram. Soc. Jpn. 102 (1994) 530.
[13] S. Hayakawa, T. Yoko, S. Sakka, J. Solid State Chem. 112 (1994) 329.
[14] O.N. Antzutkin, S.C. Shekar, M.H. Levitt, J. Magn. Reson., Ser. A 115 (1995) 7.
[15] M. Menetrier, A. Rougier, C. Delmas, Solid State Commun. 90 (1994) 439.
[16] C. Marichal, J. Hirschinger, P. Granger, M. Menetrier, A. Rougier, C. Delmas, Inorg. Chem. 34 (1995) 1773.
[17] M. Carewska, S. Scaccia, F. Croce, S. Arumugam, Y. Wang, S. Greenbaum, Solid State Ionics 93 (1997) 227.
[18] J. Sugiyama, T. Atsumi, A. Koiwai, T. Sasaki, T. Hioki, N. Kamegashira, J. Phys.: Condens. Matter 9 (1997) 1729.
[19] C.A. Fyfe, Solid State NMR for Chemists,1983.